# Wetting and drying of a rigid substrate under variation of the microscopic details

C. Bruin

*Laboratorium voor Technische Natuurkunde, Technische Universiteit Delft*
*P.O. Box 5046, 2600 GA Delft, the Netherlands*

Wetting and drying of a rigid substrate by a Lennard-Jones fluid in molecular dynamics simulations is reported. The size of the substrate particles, being smaller than the fluid particles in former simulations, is now taken to be equal to, respectively larger than, that of the fluid particles. Recently, for the latter type of system a first order drying transition has been reported. Like before we find a continuous-like transition for all systems considered. This also holds for substrates with incompletely-filled top layers, the so-called molecularly rough surfaces. All systems studied behave qualitatively alike, but inconsistencies are found in the solid-vapour surface tension on approach of the wetting transition and for the solid-fluid surface tension in general.

*Key words:* wetting, drying, molecular dynamics
*PACS:* 68.45.Gd, 68.10.Cr, 61.20.CA

## 1 Introduction

In a recent molecular dynamics (MD) paper of fluid wetting on molecularly rough surfaces, Tang and Harris [1] present also results for the drying transition on a molecularly smooth surface. These results suggest a first order drying transition and even a metastable partially-dry state as a value of $\cos\theta$ significantly smaller than -1 is reported. The rigid substrate consists of static particles on an FCC lattice. The smooth-surface substrate contains three (100) layers. For the rough surface a partially-filled (100) layer is added on both sides of the substrate. For the evaluation of the contact angle $\theta$, Young's relation has been applied [2]

$$\cos\theta = (\gamma_{sv} - \gamma_{sl})/\gamma_{lv}, \tag{1}$$

where $\gamma_{ij}$ is the surface tension of the interface between phases $i$ and $j$ and the subscripts $s$, $l$ and $v$ denote the solid, liquid and vapour phase, respectively.

In a Comment [3] we have objected against the Tang and Harris expression for $\gamma_{sf}$, where $f$ stands for fluid (either liquid or vapour). Harris has complied with our objection in his Reply [4]. After correction, the above-mentioned result for $\cos\theta$ remains and is at variance with results obtained by us before [5]. From our results, we concluded [5] the drying transition to be continuous or very weakly first order. Because of this discrepancy, we performed MD simulations on the Tang and Harris smooth- and rough-surface systems. A system with fluid and solid particles of equal size (in between our original system and the Tang and Harris system) has been studied too.

Another reason for reexamining the systems studied by Tang and Harris [1] is the surprising behaviour of $\gamma_{sv}$, that turns out not to decrease monotonously with increasing substrate-fluid interaction parameter $\epsilon_{sf}$, even so after correction [4]. The derivative $\partial\gamma_{sv}/\partial\epsilon_{sf}$ can be determined directly in the simulations and was always found to be negative in our previous simulations. This derivative has not been reported by Tang and Harris.

We start out in section 2 with a survey of the systems studied. In section 3 we present results for the contact angle, $\cos\theta$, and its derivative $\partial\cos\theta/\partial\epsilon_r = \epsilon_{ff}\partial\cos\theta/\partial\epsilon_{sf}$. The substrate-fluid surface tensions are shown in section 4 and discrepancy with their derivatives is exposed. As a check on internal consistence we present data on the liquid-vapour surface tension, the pressure and the liquid and the vapour density in section 5. We end up with a summary of our conclusions in section 6. In the Appendix Table 3 contains the essential drying/wetting data.

## 2 Description of the systems simulated

The systems we simulate contain both substrate and fluid particles that interact through a truncated and shifted Lennard-Jones (LJ) potential

$$\Phi_{AB}(r) = \begin{cases} \phi_{AB}(r) - \phi_{AB}(r_c), & r \le r_c \\ 0, & r > r_c \end{cases} \tag{2}$$

with $\phi_{AB}(r) = 4\epsilon_{AB}\{(\sigma_{AB}/r)^{12} - (\sigma_{AB}/r)^6\}$, where $A$ and $B$ stand for either "substrate" or "fluid", $r$ denotes the distance between the particles, $\epsilon_{AB}$ sets the energy scale and $\sigma_{AB}$ the length scale of the potential. The cut-off radius is $r_c = 2.5\sigma_{AB}$. We have used the same program as before [5], although the "massive stochastic collisions" method of Tang and Harris [1] has been checked as well. For our expressions of the surface tensions $\gamma_{sf}$ and $\gamma_{lv}$, as integrals over pressure tensor components, we refer to Nijmeijer et al. [6,7]. For the

Table 1
Summary of the systems simulated for $\sigma^*_{sf} = 1.0$ and $\sigma^*_{sf} = 1.1$ for smooth (sm) substrates, and for rough substrates for $\sigma^*_{sf} = 1.1$ with coverage of the top layers 1/4 (r1), 2/4 (r2) and 3/4 (r3) respectively. $N_c$ denotes the number of unit cells of the substrate both in the $x$- and $y$-direction and the third column gives the resulting linear dimensions ( $L^*_x = L^*_y$ ). The next entries give the length of the system $L^*_z$ perpendicular to the substrate, the number of substrate particles ($N_s$) and the number of fluid particles ($N_f$) respectively. The number of time steps per run is given: $\Delta t$/run, where the number of runs ranges from fifty up to eight hundred (for slowly equilibrating systems). The liquid-vapour surface tension is given in the last column.

| system | $N_c$ | $L^*_x = L^*_y$ | $L^*_z$ | $N_s$ | $N_f$ | $\Delta t/run$ | $\gamma^*_{lv}$ |
|---|---|---|---|---|---|---|---|
| sm | | | | | | | $\sigma^*_{sf} = 1.0$ |
| S3 | 5 | 7.94 | 38 | 150 | 816 | 60000 | 0.239(2) |
| S2 | 10 | 15.87 | 38 | 600 | 3264 | 15000 | 0.231(1) |
| S1 | 20 | 31.75 | 38 | 2400 | 13056 | 4000 | 0.227(3) |
| sm | | | | | | | $\sigma^*_{sf} = 1.1$ |
| S3 | 4 | 7.62 | 38 | 96 | 752 | 60000 | 0.243(2) |
| S2 | 8 | 15.24 | 38 | 384 | 3008 | 15000 | 0.231(1) |
| S1 | 16 | 30.48 | 38 | 1536 | 12032 | 4000 | 0.229(3) |
| r1 | | | | | | | $\sigma^*_{sf} = 1.1$ |
| S2 | 8 | 15.24 | 41 | 448 | 3008 | 15000 | 0.233(1) |
| S1 | 16 | 30.48 | 41 | 1792 | 12032 | 4000 | 0.232(2) |
| r2 | | | | | | | $\sigma^*_{sf} = 1.1$ |
| S2 | 8 | 15.24 | 41 | 512 | 3008 | 15000 | 0.231(1) |
| S1 | 16 | 30.48 | 41 | 2048 | 12032 | 4000 | 0.228(4) |
| r3 | | | | | | | $\sigma^*_{sf} = 1.1$ |
| S2 | 8 | 15.24 | 41 | 576 | 3008 | 15000 | 0.229(1) |
| S1 | 16 | 30.48 | 41 | 2304 | 12032 | 4000 | 0.222(6) |

relation between the derivative $\partial\gamma_{sf}/\partial\epsilon_{sf}$ and the potential energy $U_{sf}$ of the substrate-fluid interaction we refer to references [5,7–9], $U_{sf}$ is calculated for each side of the substrate separately.

As before [5], all systems have been studied at a constant temperature $T^* = k_BT/\epsilon_{ff} = 0.9$, that was kept fixed by scaling the velocities of the fluid particles every hundredth time step. For the integration of the equations of mo-

tion the leap-frog algorithm has again been used with a reduced time step $\Delta t^* = \Delta t\sqrt{\epsilon_{ff}}/(\sigma_{ff}\sqrt{m_f}) = 0.01$, where $m_f$ denotes the mass of a fluid particle. Every twentieth time step a configuration is used for the calculation of the surface tensions and the substrate-fluid potential energies, as well as the density profiles. The key parameter determining drying/wetting behaviour is the interaction parameter $\epsilon_{sf}$ in units of $\epsilon_{ff} : \epsilon_r = \epsilon_{sf}/\epsilon_{ff}$.

In Table 1 the characteristics of the various systems are given. System S3 for $\sigma^*_{sf} = \sigma_{sf}/\sigma_{ff} = 1.1$, labeled "$\sigma$11-sm", is identical to the smooth-surface system of Tang and Harris [1,4], except for the length $L^*_z$ of the system. From their specifications $\sigma^*_{ss} = 1.2$ and $L^*_x = L^*_y = 7.62$, with 4 unit cells lateral in the substrate, we derive the nearest-neighbour distance in the substrate to be the position of the minimum of the LJ potential. It turns out that these interface dimensions are rather close to those of the system S3 for $\sigma^*_{sf} = 0.941$ ($\sigma^*_{ss} = 0.833$), with 6 lateral unit cells, in our former paper [5]: $L^*_x = L^*_y = 7.94$. The dimensions of the other smooth-surface system mentioned in Table 1, $\sigma^*_{sf} = 1$ ($\sigma^*_{ss} = 1$) with 5 lateral unit cells, are identical: $L^*_x = L^*_y = 7.94$. Therefore we denote all three systems with "S3", to specify the size of the interface area. As before, it is necessary to study larger interface area's as well, where S2 has a 4 times larger and S1 has a 16 times larger surface area (see also [5]). For the rough-surface systems of Tang and Harris, with incompletely-filled extra top layers on both sides of the substrate, only our results for the larger systems are mentioned. For the different system sizes the number of time steps per run is such that the statistical accuracy and the CPU time per run are about constant. For the last column of Table 1 the liquid-vapour surface tension $\gamma^*_{lv} = \gamma_{lv}\sigma^2_{ff}/\epsilon_{ff}$ has been averaged over all $\epsilon_r$ values for the pertaining system. The numbers between parentheses denote the uncertainty (one standard deviation) in the last one or two digits.

## 3 Results of the simulations for $\cos\theta$

The results of the simulations, regarding $\gamma^*_{sl}$, $\gamma^*_{sv}$ and $\cos\theta$ and their derivatives with respect to $\epsilon_r$, or rather $\epsilon_{sf}$, are listed in the Table 3 in the Appendix. In Fig. 1, $\cos\theta$ for three smooth-surface systems and one rough-surface system is shown. The results of the two omitted rough-surface systems $\sigma$11-r1 and $\sigma$11-r3 are rather close to those of the smooth-surface system $\sigma$11-sm. Our earlier results for $\sigma^*_{sf} = 0.941$ ($\sigma$94) are represented by a thick full line. It is taken from [5], where its origin is explained (multi-histogram method for $\epsilon_r \leq 0.25$ and cubic spline fit for $\epsilon_r > 0.25$) and it is shown to represent very well the various systems reported there. For completeness two data around the wetting transition have been added (circles, system S33 [5], that has a liquid phase doubled in the $z$-direction with respect to S3). Comparing the various systems we conclude that variation of the microscopic details of the

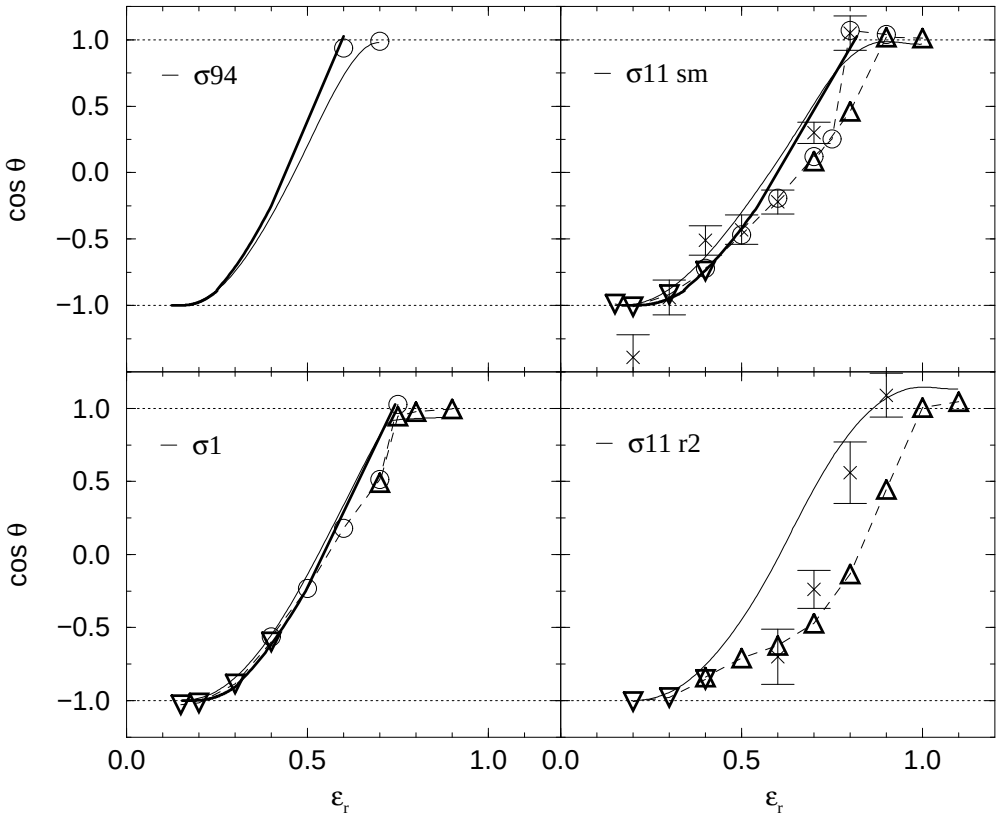


Fig. 1. $\cos\theta$ as a function of $\epsilon_r$. Dotted lines at 1 and -1 denote the completely-wet and completely-dry values of $\cos\theta$ respectively. Results for the various system sizes are denoted by O (S3), $\triangle$ (S2) and $\bigtriangledown$ (S1). Error bars have been omitted as they are smaller than the symbol size. Dashed lines connecting the symbols should guide the eye. Thin full lines result from integrating spline fits, to $\partial\cos\theta/\partial\epsilon_r$ (Fig.2). Thick full lines represent the results for $\sigma 94$ [5], and the scaled versions (see text) for $\sigma 1$ and $\sigma 11$-sm respectively. The corrected Tang and Harris data (crosses) have error bars of two standard deviations.

substrate does not effect the qualitative behaviour of drying and wetting, as expected. For the smooth-surface systems, increasing $\sigma_{sf}$ (and thereby $\sigma_{ss}$) gives the same behaviour at larger values of $\epsilon_r$. The external potential, that the substrate imposes on the fluid, can be approximated by summing over all substrate particles and averaging over the directions parallel to the surface. This external potential gets less deep for increasing $\sigma_{ss}$, due to the lower density of the substrate, but it has a larger range due to a larger $\sigma_{sf}$. From the integrated negative part of the external potentials, scaling factors can be deduced for $\epsilon_r$, 1.24 for $\sigma 1$ and 1.36 for $\sigma 11$-sm, with respect to $\sigma 94$. Both scaled results, of $\sigma 94$, are shown in Fig. 1 by thick full lines too.

For reasons we will discuss later, we have exploited another route as well to obtain $\cos\theta$ ( and $\gamma^*_{sl}$ and $\gamma^*_{sv}$). As we have calculated also $\partial\gamma^*_{sl}/\partial\epsilon_r$ and $\partial\gamma^*_{sv}/\partial\epsilon_r$, we have made spline fits for these quantities and for $\partial\cos\theta/\partial\epsilon_r$

(see also Fig.2) and have integrated these fits. For the systems mentioned in Table 1 we have taken together data for the various surface area's, in case of overlapping data we always dropped the data belonging to smaller surface area's. For system $\sigma 94$ we took the data of D1, special purpose computer system of size S1 [5], extended with two data points of S33 ($\epsilon_r = 0.6$ and 0.7). The results from the integration of the spline fits to $\partial \cos\theta / \partial \epsilon_r$ are shown by the thin full lines in Fig.1, where a trivial integration constant of -1 has been added. Integrating the fits to $\partial \gamma^*_{sl}/\partial \epsilon_r$ and $\partial \gamma^*_{sv}/\partial \epsilon_r$ (see section 4) to obtain $\gamma^*_{sl}$ and $\gamma^*_{sv}$ and combining the resulting surface tensions according to eq.(1) gives the same curves. The integration constants are less trivial here and we preferred to adjust the surface tensions at the lowest value of $\epsilon_r$ (see Fig.3 and 4). For $\sigma$11-sm in Fig.1 the thin full line is in much better agreement with the thick full line than the data points are. In general, we can conclude that this procedure of scaling $\epsilon_r$ accounts for the main effect of the increase of $\sigma_{sf}$, and $\sigma_{ss}$.

A striking difference between Harris's data and ours (for $\sigma$11-sm) is at $\epsilon_r = 0.2$, where he obtains $\cos\theta = -1.39(17)$, well below the completely-dry value of -1, the error bar being two standard deviations. This value is obtained with a $\gamma^*_{lv} = 0.191$, which is much lower than the value 0.234(2) we obtained for this system size (S3,[5]). Substituting the latter value of $\gamma^*_{lv}$, one obtains $\cos\theta = -1.14$ that is still too low, but that does not rule out the value -1 in view of the error bar. Another difference is that Harris finds an incompletely-dry state for $\epsilon_r = 0.3$ for the system size S3. We also simulated S3 for $\epsilon_r = 0.3$ and found the liquid phase to detach from the substrate, like we found for S3 ($\sigma 94$,[5]) for $\epsilon_r = 0.275$. For this reason we studied a 16 times larger surface area (S1) for $\epsilon_r \leq 0.4$. The reason for the above-mentioned discrepancy lies in the different way of keeping the temperature constant. We also tried Tang and Harris's method of "massive stochastic collisions" for system S3 ($\sigma$11-sm) and found $\cos\theta = -1.00(2)$ for $\epsilon_r = 0.2$. However, both the liquid density $n^*_l$ and $\gamma^*_{lv}$ become too small and the vapour density $n^*_v$ becomes too large, as Tang and Harris find too [1]. In our opinion this originates from the fact that the tendency of the liquid phase to detach from the substrate is frustrated by assigning "random" velocities to the fluid particles every 500th time step.

Another interesting feature shown in Fig.1 is the size dependence of the wetting transition for $\sigma$11-sm. System S3 becomes completely-wet for $\epsilon_r = 0.8$ (in accordance with Harris's result), where for S2 $\epsilon_r = 0.9$ applies. For $\sigma 1$ this size dependence is marginal or absent ($\epsilon_r = 0.75$) and for $\sigma 94$ we found no indication for it at all [5]. For the rough-surface systems ($\sigma 11$), the size dependence is present as well, and even more pronounced; because of the behaviour of $\gamma^*_{sv}$ (to be discussed later), we did not pursue the simulations of S3 for the rough substrates.

In Fig. 2 the derivative $\partial \cos\theta / \partial \epsilon_r$ is shown for the same simulations depicted

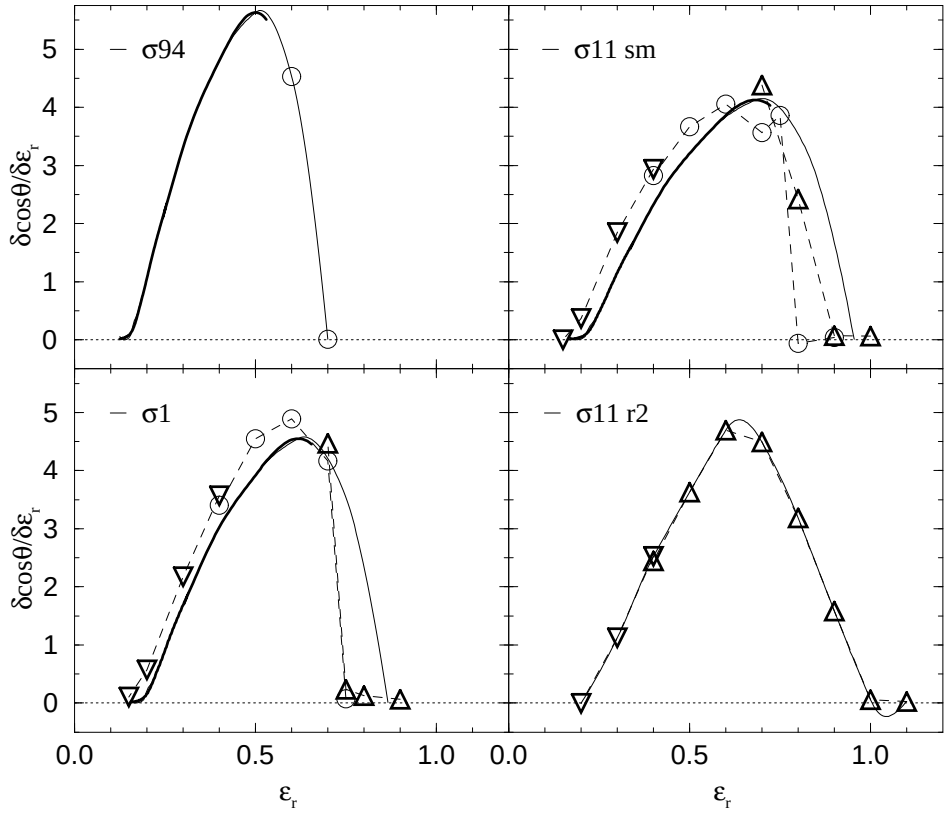


Fig. 2. $\partial \cos\theta/\partial\epsilon_r$ as a function of $\epsilon_r$ for the same systems depicted in Fig.1. The dotted line at zero gives both the completely-dry and the completely-wet value of $\partial \cos\theta/\partial\epsilon_r$. For $\sigma$94 the thick full line represents the results and the thin full line is the spline fit, see Fig.1. Both lines have been scaled for $\sigma$1 and $\sigma$11-sm. For $\sigma$11-r2 the full line represents its spline fit.

in Fig. 1. The size dependence of the wetting transition for $\sigma$11-sm manifests itself very clearly. For system size S3, $\partial \cos\theta/\partial\epsilon_r$ falls from 4 to 0 (the completely-wet value) going from $\epsilon_r = 0.75$ to $\epsilon_r = 0.8$. System size S2 gets completely wet for $\epsilon_r = 0.9$, see also Fig.1. The value of $\partial \cos\theta/\partial\epsilon_r$ at $\epsilon_r = 0.8$ looks suspicious, lying in between the top value and the completely-wet value zero. Indeed of the probes for equilibrium, $\partial\gamma^*_{sv}/\partial\epsilon_r$ and $\partial\gamma^*_{sl}/\partial\epsilon_r$, the first one shows considerable fluctuations with time, as we also found for other systems on approach of the wetting transition. Therefore we followed this system for 5.25x10$^6$ time steps after an equilibration time of 7.5x10$^5$ time steps. For comparison: S2 at $\epsilon_r = 0.9$ became completely wet after 4.5x10$^6$ time steps and was followed for 1.5x10$^6$ time steps afterwards. The scaling of $\epsilon_r$ for $\sigma$94 to $\sigma$1 and to $\sigma$11-sm, mentioned above for $\cos\theta$, should be accompanied here with scaling down $\partial \cos\theta/\partial\epsilon_r$ with the same factor. The spline fit to $\partial \cos\theta/\partial\epsilon_r$ for $\sigma$94 (using the same systems as for $\cos\theta$) is shown by the thin full line, only visible for $\epsilon_r > 0.5$. This fit has been scaled as well into results for $\sigma$1 and $\sigma$11-sm, these are also represented by thin full lines. From the comparison of the scaled data with the measured data for $\sigma$1 and $\sigma$11-sm we conclude that

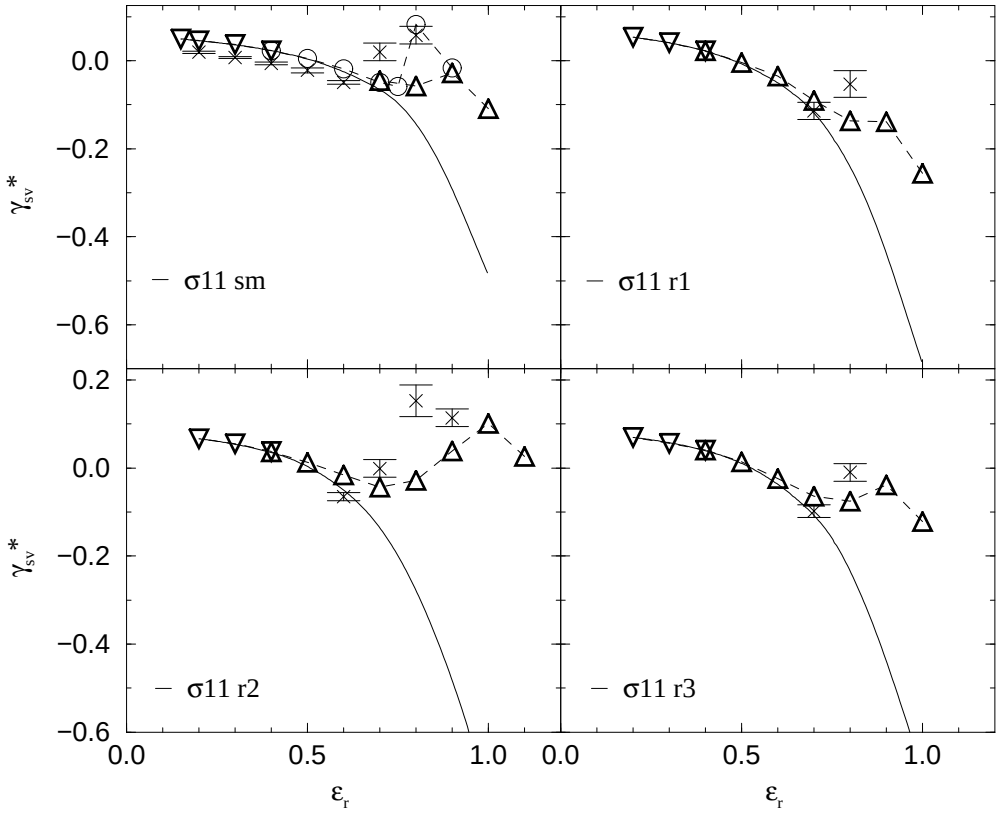


Fig. 3. $\gamma^*_{sv}$ for the various systems with $\sigma^*_{sf} = 1.1$. Results for the various system sizes are denoted by O (S3), $\triangle$ (S2) and $\bigtriangledown$ (S1). Error bars have been omitted as they are smaller than the symbol size. Dashed lines connecting the symbols should guide the eye. The corrected Tang and Harris data (crosses) have error bars of two standard deviations. Full lines result from integrating the spline fits to $\partial\gamma^*_{sv}/\partial\epsilon_r$ (see Fig.6).

this scaling gives a reasonable estimate of the effect of increasing $\sigma_{sf}$, and $\sigma_{ss}$. It should be noted that the thin full line for $\sigma$11-r2 in Fig.2 represents the spline fit to the data and this fit has been integrated to obtain $\cos\theta$ in Fig.1 for $\sigma$11-r2.

## 4 Surface tensions

In Fig.3 the results of $\gamma^*_{sv}$ for the various systems with $\sigma^*_{sf} = 1.1$ are shown. The data of Harris [4] all show an increase of $\gamma^*_{sv}$ with increasing $\epsilon_r$ on approach of the wetting transition (system size S3). In our previous simulations [5] for $\sigma$94 we never encountered such a behaviour for any system size.

For the smooth-surface system ($\sigma$11-sm), behaviour comparable to that of the data of Harris is shown by system S3, although $\gamma^*_{sv}$ is decreasing up to

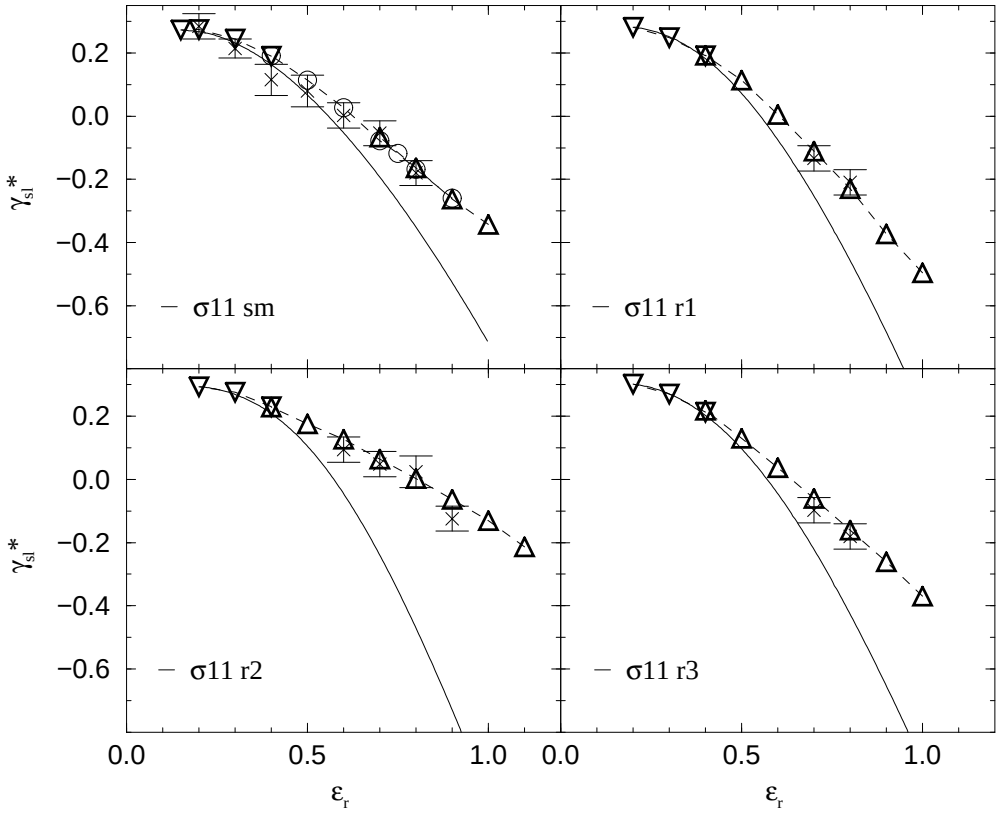


Fig. 4. $\gamma^*_{sl}$ for the various systems with $\sigma^*_{sf} = 1.1$ (see Fig.3). Full lines result from integrating the spline fits to $\partial\gamma^*_{sl}/\partial\epsilon_r$ (see Fig.6).

$\epsilon_r = 0.75$. For $\epsilon_r = 0.8$, the same completely-wet state is found. The increase of $\gamma^*_{sv}$ for S2, with a larger interface area, is less prominent ($\epsilon_r = 0.9$), but does exist. It looks like the system jumps to the completely-wet branch, that is really $\gamma^*_{sl} + \gamma^*_{lv}$, at a too low value of $\epsilon_r$. So we performed simulations for S1 as well in this region, but we still found the tendency of $\gamma^*_{sv}$ to increase, although the exceptional long equilibration times prevented us from arriving at a fully equilibrated completely-wet state for such a large system. From the rough-surface systems, $\sigma$11-r1 and $\sigma$11-r3 show very much the same behaviour as the smooth-surface system, which also holds for the few data of Harris. The situation for $\sigma$11-r2, that becomes completely wet at $\epsilon_r = 1$, looks different as the increase of $\gamma^*_{sv}$ takes place over a much larger range: $0.7 < \epsilon_r < 1$. The increase of $\gamma^*_{sv}$ just before the wetting transition, and for $\sigma$11-r2 in a larger region, is in contradiction with $\partial\gamma^*_{sv}/\partial\epsilon_r$ as depicted in Fig.6, being always negative and getting more negative for increasing $\epsilon_r$. We therefore made spline fits to this derivative (see Fig.6). Integration of the spline fits, taking the integration constant such that values at low $\epsilon_r$ match the directly measured data, results in the full lines of Fig.3. The agreement up to $\epsilon_r \approx 0.6$ is good, but it gets dramatically bad for higher values of $\epsilon_r$.

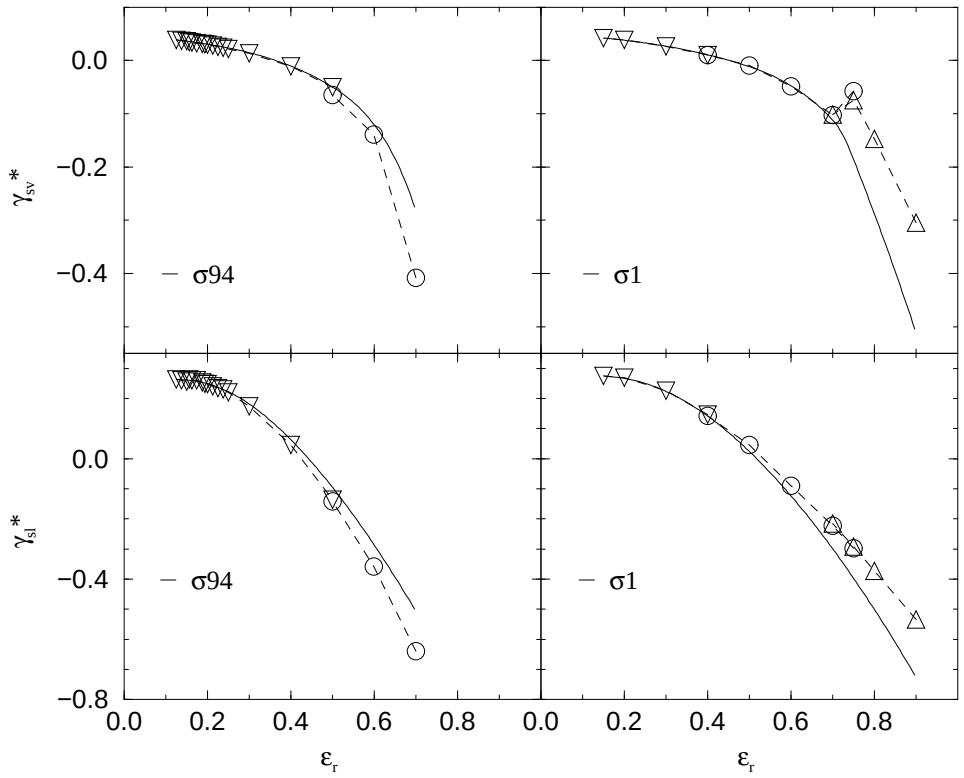


Fig. 5. $\gamma^*_{sv}$ for the smooth-surface systems $\sigma 94$ and $\sigma 1$ (two upper graphs), and $\gamma^*_{sl}$ (two lower graphs). Full lines denote the integrated spline fits of the respective derivatives. Symbols for $\sigma 1$ are according to Fig.3. For $\sigma 94$ data of D1 ($\bigtriangledown$) and S33 (circles) are given.

In Fig.4 $\gamma^*_{sl}$ is shown for the same systems. There is very good agreement with the data of Harris (crosses). The data look much more regular here, and of course nothing special is happening to $\gamma^*_{sl}$ on approach of the wetting transition. However, applying the same procedure of integrating now the spline fits to $\partial\gamma^*_{sl}/\partial\epsilon_r$ (Fig.6), resulting in the full lines, also shows a large discrepancy with the directly measured surface tensions. The discrepancy is even starting at lower values of $\epsilon_r$. One should note that at these low values of $\epsilon_r$, $\gamma^*_{sl}$ is affected by the build-up of the liquid phase near the substrate (for increasing $\epsilon_r$). The same phenomenon applies to $\gamma^*_{sv}$ on approach of the wetting transition. We calculated the two contributions to $\gamma^*_{sf}$ (referring to both $\gamma^*_{sv}$ and $\gamma^*_{sl}$) separately, i.e. the fluid-fluid and the substrate-fluid part. They have opposite signs and their absolute values become five to ten times larger for $\gamma^*_{sv}$ than the quantity itself in the completely-wet region. However, no suspect behaviour could be found for the constituents. A possible reason, for the discrepancy between $\gamma^*_{sf}$ and its derivative $\partial\gamma^*_{sf}/\partial\epsilon_r$, is registration of the fluid particles onto the substrate, that is excluded for system $\sigma 94$. We tried to check this conjecture by visual inspection of the first few liquid layers nearest to the

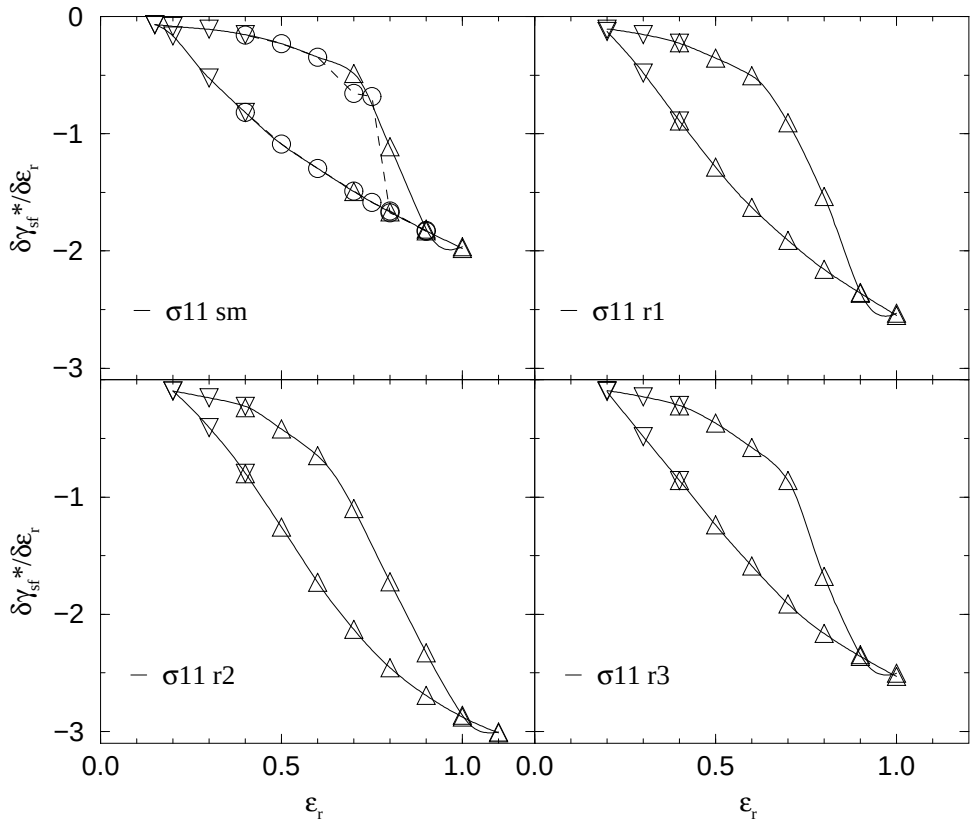


Fig. 6. $\partial\gamma^*_{sv}/\partial\epsilon_r$, upper curves, and $\partial\gamma^*_{sl}/\partial\epsilon_r$, lower curves, for the various systems with $\sigma^*_{sf} = 1.1$ (see Fig.3 and 4). Full lines show the spline fits to the data, that have been integrated to obtain $\gamma^*_{sv}$ and $\gamma^*_{sl}$ (also full lines) in Fig.3 and Fig.4 respectively.

substrate, but did not find evidence for it. A quantitative analysis, through a pair distribution function or a (two-dimensional) structure factor, should be decisive.

We observe the discrepancy growing, with the substrate becoming less smooth, as it does when the substrate particles become larger. For $\sigma$94 [5] we find a small discrepancy (see Fig.5), that has opposite sign with respect to the discrepancies displayed in Fig.3 and 4. For $\sigma$1 the particle sizes are equal and we find a relatively small discrepancy (see Fig.5). For $\sigma$11-sm the substrate particles are larger than the fluid particles, and the discrepancy is large (Fig.3 and 4). For $\sigma$11-r1 and for $\sigma$11-r3 the discrepancy is about the same as for $\sigma$11-sm. Apparently both systems, with a top layer of the substrate consisting for one quarter out of particles and for one quarter out of vacancies respectively, do not look rougher to the fluid than $\sigma$11-sm does. One could argue that $\sigma$11-r2, with a 50% filled top layer, looks rougher than $\sigma$11-sm and can be supposed to favour registration even more, the discrepancy is larger indeed (see Fig.3 and 4).

In Fig.6 the derivatives $\partial\gamma^*_{sv}/\partial\epsilon_r$ and $\partial\gamma^*_{sl}/\partial\epsilon_r$ are shown, together with the

spline fits. The different systems show very much the same behaviour. It should be noted however that, considering systems $\sigma$11-sm, $\sigma$11-r3, $\sigma$11-r1 and $\sigma$11-r2, and in that order, $\partial\gamma^*_{sv}/\partial\epsilon_r$ (upper curves) starts to decrease more rapidly at lower values of $\epsilon_r$ and shows a smoother overall behaviour.

## 5 Liquid-vapour equilibrium

As there are always coexisting liquid and vapour phases in our simulations with at least one interface in between, we obtained quite some data on the liquid density $n^*_l$, the vapour density $n^*_v$ and the pressure $p^*$ at coexistence ($T^* = 0.9$), as well as on the liquid-vapour surface tension $\gamma^*_{lv}$. As a check on the consistence of our simulations and possibly as a reference, the numbers are given in Table 2.

In Table 1 we already presented values for $\gamma^*_{lv}$ for the various systems. We average these values for the various system sizes separately and find $\gamma^*_{lv}$ to depend on the size of the surface area (Table 2), like we reported before [5], where the value for S3 (0.236) differs slightly from the one mentioned in [5] (0.234) because of other weight factors. For completeness we mention the result for a system (S0) with a 4 times larger interface area [5] than S1: $\gamma^*_{lv} = 0.227(1)$, that fits in quite nicely with the results obtained here. Two other relatively recent results are from Adams and Henderson [10] for a system with a bit smaller interface area than S3: $\gamma^*_{lv} = 0.23(1)$, and Haye and Bruin [11]: $\gamma^*_{lv} = 0.223(3)$ S1. For the calculation of $\cos\theta$ with eq.(1) we used the same values of $\gamma^*_{lv}$ as before [5]. The discrepancy of a few percent between the old value for S3 and the present one has been ignored.

For the pressure our present results suggest size dependence as well, as it is increasing with system size; the error bars prevent us from drawing this conclusion. Moreover, it is not supported by the data of our previous work. For system size S0 we obtained $p^* = 0.03130(1)$, Adams and Henderson [10] report: $p^* = 0.0322(13)$ and Haye and Bruin [11]: $p^* = 0.0308(2)$.

Size dependence can be excluded for the coexisting densities. We note quite a discrepancy with our previous work for the liquid densities. System D1 shows the largest discrepancy. In the old results for S3, S2, and S1, systems with a doubled liquid phase (S33, S22 and S11 see ref. [5] ) are included and the numbers are in between that for D1 and the present results. The average for $n^*_l$ over S33, S22 and S11 alone is given in the last column and is in good agreement with the present result. Since we took narrower boundaries for the determination of the liquid density in the present simulations and since more fluid particles resided in the liquid phase than for D1, S3, S2, S1 and S0 in our previous simulations, we can understand the different outcomes. Furthermore

Table 2
Liquid-vapour coexistence data at $T^* = 0.9$ for the various system sizes. Each row with present results is followed by one with previous results [5] for the same quantity. The last column contains the average value, where appropriate. In the average value for $n_l^*$ [5] only the results of the doubled liquid phase systems S33, S22 and S11 have been taken into account (see text).

| | S3 | S2 | S1 | D1 | <> |
|---|---|---|---|---|---|
| $\gamma_{lv}^*$ | 0.241(2) | 0.231(1) | 0.228(2) | | |
| [5] | 0.236(2) | 0.229(3) | 0.226(1) | 0.225(1) | |
| $p^*$ | 0.03109(8) | 0.03122(4) | 0.03138(7) | | 0.03124(3) |
| [5] | 0.0313(2) | 0.0313(1) | 0.03136(6) | 0.03102(5) | 0.03122(3) |
| $n_l^*$ | 0.6646(2) | 0.6643(1) | 0.6645(1) | | 0.6644(1) |
| [5] | 0.6635(4) | 0.6631(5) | 0.6631(5) | 0.6622(1) | 0.6645(1) |
| $n_v^*$ | 0.0446(2) | 0.0449(1) | 0.0450(2) | | 0.0449(1) |
| [5] | 0.0452(3) | 0.0453(3) | 0.0453(2) | 0.0457(1) | 0.0452(1) |

Adams and Henderson (see above) report: $n_l^* = 0.671(1)$ and $n_v^* = 0.040(3)$ and Haye and Bruin (see above): $n_l^* = 0.6619(4)$ and $n_v^* = 0.0454(4)$. For the liquid density these results are much higher respectively much lower than our present result. We note that for $< n_v^* >= 0.0452$ in the last row, the S0 result ($n_v^* = 0.0450(1)$) has been taken into account as well. The measured value for the temperature, kept fixed only approximately, equals the prescribed value of 0.9 with an accuracy that is better by a few decimals than the accuracies of the quantities mentioned above.

## 6 Conclusions

Changing the microscopic details of the substrate does not change the qualitative behaviour of drying and wetting. The quantitative change of drying and wetting for the smooth substrates, due to enlarging the size of the substrate particles, can be described reasonably well for $\cos\theta$, as it is calculated from its derivative, by matching the (approximate) external potentials.

The substrate-vapour surface free energy increases at, or just before, the wetting transition which seems unphysical. Discrepancy is found between the behaviour of both $\gamma_{sv}^*$ and $\gamma_{sl}^*$ and their derivatives. The discrepancy gets larger for larger substrate particles and for more roughness of the substrate. A conjecture, that registration of the fluid particles onto the substrate is responsible for this discrepancy, could not be confirmed by visual inspection and

still awaits a quantitative analysis (pair distribution or structure factor).

Dependence of the liquid-vapour surface tension on the size of the interface area has been established with better accuracy than before. Accurate numbers have been found for the coexisting vapour and liquid densities and the pressure ($T^* = 0.9$), also ensuring internal consistence of the simulations.

**Acknowledgement**

I thank Marco Nijmeijer for his inspiring interest in the present work and for his fruitful collaboration in the project, started by Hans van Leeuwen.

**Appendix**

Table 3: Surface tension results for the systems with a smooth substrate (sm), $\sigma^*_{sf} = 1.0$ and $\sigma^*_{sf} = 1.1$, and with a rough substrate (r1, r2 and r3) for $\sigma^*_{sf} = 1.1$, with coverage 1/4, 2/4 and 3/4 respectively. In the last column $\partial \cos\theta$ is a short-hand notation for $\partial \cos\theta / \partial \epsilon_r$.

| $\epsilon_r$ | $\gamma^*_{sl}$ | $\gamma^*_{sv}$ | $\cos\theta$ | $\partial\gamma^*_{sl}/\partial\epsilon_r$ | $\partial\gamma^*_{sv}/\partial\epsilon_r$ | $\partial\cos\theta$ |
|---|---|---|---|---|---|---|
| S2 | $\sigma^*_{sf} = 1$ | sm | | | | |
| 0.90 | -0.534(5) | -0.304(4) | 1.00(3) | -2.370(3) | -2.355( 4) | 0.07( 3) |
| 0.80 | -0.372(4) | -0.148(3) | 0.98(2) | -2.130(3) | -2.102( 3) | 0.12( 2) |
| 0.75 | -0.293(3) | -0.075(2) | 0.95(2) | -2.005(2) | -1.951( 3) | 0.23( 2) |
| 0.70 | -0.215(3) | -0.101(1) | 0.49(1) | -1.880(2) | -0.852( 9) | 4.47( 4) |
| S3 | $\sigma^*_{sf} = 1$ | sm | | | | |
| 0.75 | -0.298(4) | -0.058(4) | 1.03(2) | -2.005(4) | -1.987( 5) | 0.08( 3) |
| 0.70 | -0.222(4) | -0.102(2) | 0.51(2) | -1.870(3) | -0.896(24) | 4.16(11) |
| 0.60 | -0.091(6) | -0.048(2) | 0.18(3) | -1.612(6) | -0.467(19) | 4.89( 9) |
| 0.50 | 0.045(6) | -0.010(1) | -0.23(3) | -1.325(5) | -0.261( 8) | 4.55( 4) |
| 0.40 | 0.142(7) | 0.010(1) | -0.56(3) | -0.989(6) | -0.192( 7) | 3.41( 4) |
| S1 | $\sigma^*_{sf} = 1$ | sm | | | | |

Table 3: continued

| $\epsilon_r$ | $\gamma^*_{sl}$ | $\gamma^*_{sv}$ | $\cos\theta$ | $\partial\gamma^*_{sl}/\partial\epsilon_r$ | $\partial\gamma^*_{sv}/\partial\epsilon_r$ | $\partial\cos\theta$ |
|---|---|---|---|---|---|---|
| 0.40 | 0.146(5) | 0.010(1) | -0.60(2) | -0.994(5) | -0.188( 2) | 3.57( 2) |
| 0.30 | 0.226(6) | 0.026(1) | -0.88(3) | -0.622(5) | -0.131( 2) | 2.17( 3) |
| 0.20 | 0.269(5) | 0.039(1) | -1.02(2) | -0.220(6) | -0.092( 1) | 0.57( 3) |
| 0.15 | 0.275(6) | 0.042(1) | -1.03(3) | -0.098(3) | -0.075( 1) | 0.10( 2) |
| S2 | $\sigma^*_{sf} = 1.1$ | sm | | | | |
| 1.00 | -0.342(4) | -0.109(3) | 1.01(2) | -1.978(2) | -1.964( 2) | 0.06( 2) |
| 0.90 | -0.262(4) | -0.028(3) | 1.02(2) | -1.827(2) | -1.811( 3) | 0.07( 1) |
| 0.80 | -0.164(2) | -0.058(1) | 0.46(1) | -1.667(1) | -1.110( 9) | 2.42( 4) |
| 0.70 | -0.066(3) | -0.045(1) | 0.09(1) | -1.492(2) | -0.485( 5) | 4.38( 3) |
| S3 | $\sigma^*_{sf} = 1.1$ | sm | | | | |
| 0.90 | -0.259(4) | -0.016(4) | 1.04(3) | -1.833(3) | -1.823( 3) | 0.04( 2) |
| 0.80 | -0.168(4) | 0.082(5) | 1.07(3) | -1.659(3) | -1.673( 3) | -0.06( 2) |
| 0.75 | -0.118(4) | -0.059(2) | 0.25(2) | -1.585(2) | -0.682(21) | 3.86( 9) |
| 0.70 | -0.078(6) | -0.049(2) | 0.12(3) | -1.490(3) | -0.656(25) | 3.57(11) |
| 0.60 | 0.027(5) | -0.018(1) | -0.19(2) | -1.295(3) | -0.345(13) | 4.06( 6) |
| 0.50 | 0.114(5) | 0.005(1) | -0.47(2) | -1.089(4) | -0.231( 7) | 3.67( 3) |
| 0.40 | 0.191(5) | 0.023(1) | -0.72(2) | -0.817(7) | -0.157( 3) | 2.82( 3) |
| S1 | $\sigma^*_{sf} = 1.1$ | sm | | | | |
| 0.40 | 0.190(6) | 0.022(1) | -0.74(2) | -0.818(4) | -0.154( 2) | 2.93( 2) |
| 0.30 | 0.244(6) | 0.037(1) | -0.92(3) | -0.526(6) | -0.109( 2) | 1.84( 3) |
| 0.20 | 0.274(6) | 0.046(1) | -1.01(3) | -0.165(7) | -0.082( 1) | 0.37( 3) |
| 0.15 | 0.273(4) | 0.049(1) | -0.99(2) | -0.068(1) | -0.068( 1) | 0.00( 1) |
| S2 | $\sigma^*_{sf} = 1.1$ | r1 | | | | |
| 1.00 | -0.495(5) | -0.256(5) | 1.04(3) | -2.549(3) | -2.532( 3) | 0.07( 2) |
| 0.90 | -0.372(5) | -0.139(4) | 1.02(3) | -2.360(3) | -2.352( 3) | 0.03( 2) |
| 0.80 | -0.229(3) | -0.137(1) | 0.40(2) | -2.158(2) | -1.536( 7) | 2.70( 3) |

Table 3: continued

| $\epsilon_r$ | $\gamma^*_{sl}$ | $\gamma^*_{sv}$ | $\cos\theta$ | $\partial\gamma^*_{sl}/\partial\epsilon_r$ | $\partial\gamma^*_{sv}/\partial\epsilon_r$ | $\partial\cos\theta$ |
|---|---|---|---|---|---|---|
| 0.70 | -0.111(5) | -0.091(1) | 0.09(2) | -1.909(2) | -0.904(11) | 4.37( 5) |
| 0.60 | 0.006(6) | -0.035(1) | -0.18(3) | -1.628(4) | -0.505( 9) | 4.88( 5) |
| 0.50 | 0.115(6) | -0.004(1) | -0.52(3) | -1.285(4) | -0.354( 7) | 4.05( 4) |
| 0.40 | 0.193(5) | 0.023(1) | -0.74(2) | -0.891(4) | -0.223( 4) | 2.91( 2) |
| S1 | $\sigma^*_{sf} = 1.1$ | r1 | | | | |
| 0.40 | 0.192(5) | 0.022(1) | -0.75(2) | -0.889(4) | -0.227( 2) | 2.93( 2) |
| 0.30 | 0.248(4) | 0.041(1) | -0.92(2) | -0.480(5) | -0.153( 2) | 1.45( 3) |
| 0.20 | 0.282(5) | 0.053(1) | -1.01(2) | -0.128(4) | -0.105( 1) | 0.10( 2) |
| S2 | $\sigma^*_{sf} = 1.1$ | r2 | | | | |
| 1.10 | -0.214(5) | 0.026(4) | 1.05(3) | -3.011(2) | -3.004( 2) | 0.03( 1) |
| 1.00 | -0.130(6) | 0.102(4) | 1.01(3) | -2.876(2) | -2.863( 2) | 0.06( 2) |
| 0.90 | -0.064(3) | 0.039(2) | 0.45(2) | -2.693(2) | -2.329( 5) | 1.58( 2) |
| 0.80 | 0.003(3) | -0.028(2) | -0.13(1) | -2.456(2) | -1.723( 9) | 3.18( 4) |
| 0.70 | 0.064(5) | -0.044(1) | -0.47(2) | -2.130(4) | -1.098(13) | 4.49( 6) |
| 0.60 | 0.127(7) | -0.016(1) | -0.62(3) | -1.728(6) | -0.648(10) | 4.69( 5) |
| 0.50 | 0.176(5) | 0.013(1) | -0.71(2) | -1.255(6) | -0.420( 9) | 3.63( 5) |
| 0.40 | 0.230(6) | 0.037(1) | -0.84(3) | -0.801(6) | -0.238( 5) | 2.45( 4) |
| S1 | $\sigma^*_{sf} = 1.1$ | r2 | | | | |
| 0.40 | 0.231(5) | 0.038(1) | -0.85(2) | -0.795(5) | -0.225( 3) | 2.52( 3) |
| 0.30 | 0.277(5) | 0.055(1) | -0.98(2) | -0.407(5) | -0.153( 2) | 1.12( 2) |
| 0.20 | 0.294(7) | 0.066(1) | -1.01(3) | -0.095(1) | -0.095( 1) | 0.00( 1) |
| S2 | $\sigma^*_{sf} = 1.1$ | r3 | | | | |
| 1.00 | -0.370(4) | -0.122(3) | 1.08(2) | -2.530(2) | -2.505( 2) | 0.11( 1) |
| 0.90 | -0.261(5) | -0.039(5) | 0.96(4) | -2.360(4) | -2.346( 4) | 0.06( 3) |
| 0.80 | -0.161(3) | -0.076(2) | 0.37(2) | -2.165(2) | -1.678( 6) | 2.11( 3) |
| 0.70 | -0.060(5) | -0.064(1) | -0.02(2) | -1.911(4) | -0.857(10) | 4.58( 4) |

Table 3: continued

| $\epsilon_r$ | $\gamma^*_{sl}$ | $\gamma^*_{sv}$ | $\cos\theta$ | $\partial\gamma^*_{sl}/\partial\epsilon_r$ | $\partial\gamma^*_{sv}/\partial\epsilon_r$ | $\partial\cos\theta$ |
|---|---|---|---|---|---|---|
| 0.60 | 0.037(6) | -0.024(1) | -0.26(3) | -1.587(4) | -0.577(13) | 4.39( 6) |
| 0.50 | 0.130(5) | 0.014(1) | -0.50(2) | -1.239(4) | -0.370( 8) | 3.78( 4) |
| 0.40 | 0.218(5) | 0.040(1) | -0.77(2) | -0.860(4) | -0.220( 5) | 2.78( 3) |
| S1 | $\sigma^*_{sf} = 1.1$ | r3 | | | | |
| 0.40 | 0.213(5) | 0.041(1) | -0.76(2) | -0.858(4) | -0.219( 3) | 2.83( 2) |
| 0.30 | 0.271(4) | 0.056(1) | -0.95(2) | -0.484(5) | -0.144( 2) | 1.50( 2) |
| 0.20 | 0.301(7) | 0.069(1) | -1.03(3) | -0.100(2) | -0.092( 1) | 0.04( 1) |

## References


[1] J.Z. Tang and J.G. Harris, J. Chem. Phys. 103 (1995) 8201.

[2] J.S. Rowlinson and B. Widom, Molecular Theory of Capillarity (Clarendon, Oxford, 1982).

[3] M.J.P. Nijmeijer and C. Bruin, J. Chem. Phys. 105 (1996) 4889.

[4] J.G. Harris, J. Chem. Phys. 105 (1996) 4891.

[5] C. Bruin, M.J.P. Nijmeijer and R.M. Crevecoeur, J. Chem. Phys. 102 (1995) 7622.

[6] M.J.P. Nijmeijer, C. Bruin, A.F. Bakker and J.M.J. van Leeuwen, Phys. Rev. A 42 (1990) 6052.

[7] M.J.P. Nijmeijer, C. Bruin, A.F. Bakker and J.M.J. van Leeuwen, Phys. Rev. B 44 (1991) 834.

[8] F. van Swol and J.R. Henderson, J. Chem. Soc., Faraday Trans. 2 82 (1986) 1685.

[9] J.R. Henderson, P. Tarazona, F. van Swol and E. Velasco, J. Chem. Phys. 96 (1992) 4633.

[10] P. Adams and J.R. Henderson, Mol. Phys. 73 (1991) 1383 .

[11] M.J. Haye and C. Bruin, J. Chem. Phys. 100 (1994) 556.